Modeling of Industrial Robot Kinematics Using a Hybrid Analytical and Statistical Approach

Vinh Nguyen[1]
Engineering Laboratory,
Intelligent Systems Division,
National Institute of Standards and Technology,
Gaithersburg, MD 20899
e-mail: vinh.t.nguyen@nist.gov

Jeremy A. Marvel
Engineering Laboratory,
Intelligent Systems Division,
National Institute of Standards and Technology,
Gaithersburg, MD 20899
e-mail: jeremy.marvel@nist.gov

Industrial robots are highly desirable in applications including manufacturing and surgery. However, errors in the modeling of the kinematics of robotic arms limit their positional accuracy in industrial applications. Specifically, analytical kinematic models of the robot arm suffer from errors in coefficient calibrations and the inability to account for effects including gear backlash. However, statistical modeling methods require an extensive amount of points for calibration, which is infeasible in practical industrial environments. Hence, this paper describes, develops, and experimentally validates a hybrid modeling methodology combining both analytical and statistical methods to describe the robot kinematics in an intuitive manner that is easily adaptable for small- and medium-sized industries. By formulating an explicitly described analytical kinematic model as a prior mean distribution of a Gaussian process, the prior distribution can be updated with experimental data using statistical Bayesian Inference, thus enabling more accurate description of the robot kinematics with fewer data points. The hybrid model is demonstrated to outperform an analytical model, a neural network model, and a Gaussian Process Regression model with no prior distribution in predicting both the forward and inverse kinematics of a UR5 and UR10 robot arm. Also, the error propagation of the inverse kinematic solutions is studied. In addition, the testing framework used in this work can be used as a standardized benchmark to evaluate alternative kinematic models. [DOI: 10.1115/1.4053734]

Keywords: collaborative robot, manufacturing, Bayesian inference, kinematics

1 Introduction

Industrial robots are highly desirable in industrial applications owing to their low cost, repeatability, and application flexibility [1]. Kinematic models are widely used in applications concerning the control of industrial robots including robot-assisted surgery [2], robotic welding [3], robotic milling [4], and additive manufacturing [5]. Industrial robot kinematic models are models that predict the robot end effector pose using joint angles or the required joint angles based on robot end effector pose, known as Forward Kinematics (FK) and Inverse Kinematics (IK), respectively [6]. The current state-of-the-art in developing kinematic models relies solely on using either analytical or statistical methods.

There is a plethora of analytical methods for describing industrial robot kinematics in prior literature. Kinematic modeling is a fundamental basis for all robot types including parallel robots [7,8], cable-driven platforms [9], and continuum robots [10]. However, in addition to the fact that the aforementioned papers use solely analytical models, this paper focuses on industrial robotic arms due to their widespread use and standardized implementations. The most established modeling of industrial robot kinematics is the use of the Denavit–Hartenberg (DH) parameters. The use of DH parameters involves describing each link in terms of length and twist and each joint in terms of its link offset and joint angle [11]. By using these parameters, the homogeneous transformation matrix describing the position and orientation between joints is calculated. Thus, the FK relation between the joints to the end effector pose is calculated by applying the homogeneous transformation matrices along the kinematic chain. The application of the homogeneous transformation matrix is the most commonly established approach for FK and has been used extensively in robotics literature [12–14] in addition to simultaneous joint stiffness/DH calibration [15] and direct geometric derivation for hybrid industrial/parallel robots for space applications [16]. In addition, note that Cohen et al. [17] did not use DH parameters to solve the FK problem, but rather used Hyper-dual numbers to formulate analytical 3×3 transformation matrices along the kinematic chain. In addition Lopez et al. [8] used a numerical-based algorithm to iteratively solve the FK and IK problem, though the approach was derived from analytical methods. However, solving the IK problem is more complex than FK due to nonlinearities and the existence of multiple joint solutions for a given end effector pose [18]. Existing methods for solving the IK problem include developing closed-form solutions [18,19] and the iterative inverse Jacobian-based approaches [20,21]. Notably, Fu et al. [22] used Geometric Algebra to solve the IK problem, although the method still used DH parameters. In addition, Ferrentino et al. [23] conducted an optimization search to solve the IK problem, although the method was demonstrated in simulation. However, analytical methods are limited in their approach due to calibration errors [24] and the inability to account for real-world environmental effects such as gear backlash [25].

More recently, there has been an increase in statistical methods to model the kinematics of industrial robots. Statistical methods in the context of modeling are equation forms that are not based on physical assumptions but on statistical assumptions instead [26]. Therefore, statistical methods describing industrial robot kinematics are not prone to calibration errors derived from the geometric model of a robot. For instance, a quantum behaved particle swarm

[1]Corresponding author.

Contributed by the Mechanisms and Robotics Committee of ASME for publication in the Journal of Mechanisms and Robotics. Manuscript received October 22, 2021; final manuscript received January 24, 2022; published online February 21, 2022. Assoc. Editor: Gim Song Soh.

algorithm was used to model the IK of a 7-DoF robot arm, although the study was only used in simulation [27]. In addition, Raja et al. developed a learning framework using an artificial neural network to describe the IK of an industrial robot arm on a mobile robot [28]. Neural networks have also been used for solving the FK and IK problems of a single arm of the 7-DoF YuMi [29]. Also, Reinhard et al. used a Neural network to describe the errors in the FK problem of a continuum robot, but the statistical approach was not applied to the IK problem and did not predict end effector orientation [30]. In addition, two support vector machines were used to model the kinematics of a Mitsubishi PA-10 robot arm [31]. However, a majority of the literature using statistical methods to model robot arm kinematics is only in simulation. This is because the calibration of these methods requires an extensive number of measurements, which are prohibitively time-consuming in an actual environment. In addition, statistical methods require extensive calculation times to compute a solution, which makes them infeasible for real-time control applications.

Thus, this establishes that use of only analytical or statistical methods is insufficient for accurate prediction and efficient calibration of FK and IK models of industrial robot arms. Therefore, this paper proposes a hybrid method combining both analytical and statistical methods to describe the robot kinematics. First, a closed-formed analytical model of the robot kinematics is described. The model is treated as a prior distribution of a Gaussian process. The model is then updated using Bayesian Inference with experimental data. The end result is a model that leverages analytical methods for efficient calibration while leveraging statistical methods for more accurate predictions. The proposed method is compared to alternate analytical and statistical methods using Optitrack TRIO pose measurement data of UR5 and UR10 robots. Discussion of the results is then followed by conclusions.

2 Modeling Methodology

This section describes the modeling methodology for the UR5 and UR10 robots used in this work. The closed-form analytical model is described followed by the Bayesian Inference method to update the model based on measurements.

2.1 Analytical Modeling. The UR5 and UR10 robots are used in this work due to their commonplace use in industrial applications. Note that this work leverages a previously establish closed-form FK and IK model of the UR5 and UR10 [19], which is briefly described in this paper for clarity. In addition, the closed-form expressions in this work are more explicit than previous publications, and are therefore more accessible for research publications and industrial applications. Figure 1 shows the DH parameters of a Universal Robot. Note that the UR5 and UR10 share the same FK and IK equation forms and differ only with respect to their DH parameters.

2.1.1 Forward Kinematics. According to the homogeneous transformation between joints [11], the following transformation matrix can be used to transition the position and orientation of joint $i-1$ to its consecutive joint.

$$T_{i-1}^{i} = \left[\begin{array}{ccc|c} & R_i & & P_i \\ \hline 0 & 0 & 0 & 1 \end{array}\right] \tag{1}$$

where

$$R_i = \begin{bmatrix} \cos\theta_i & -\sin\theta_i & 0 \\ \sin\theta_i\cos\alpha_{i-1} & \cos\theta_i\cos\alpha_{i-1} & -\sin\alpha_{i-1} \\ \sin\theta_i\sin\alpha_{i-1} & \cos\theta_i\sin\alpha_{i-1} & \cos\alpha_{i-1} \end{bmatrix} P_i = \begin{bmatrix} a_{i-1} \\ -d_i\sin\alpha_{i-1} \\ d_i\cos\alpha_{i-1} \end{bmatrix}$$

where Fig. 1 denotes the notation used in this work. Note that the hth row and kth columns are denoted as $T_{i-1}^{i}(h,k)$. Therefore, to calculate the homogeneous transformation matrix of the end effector of a 6-DoF UR5 or UR10 T_0^6 using the joint angles, the homogeneous transformation matrices are calculated along the kinematic chain as follows.

$$T_0^6 = T_0^1 T_1^2 T_2^3 T_3^4 T_4^5 T_5^6 \tag{2}$$

Therefore, the individual elements in the final matrix described by Eq. (2) are the closed-form solutions as a function of the joint angles for a given set of DH parameters. Thus, the elements of Eq. (2) describe the set of prior distributions that will be used in the FK solution.

2.1.2 Inverse Kinematics. Unlike the closed-form FK solution, the closed-form IK solution is solved sequentially from θ_1 to θ_5 to θ_6 to θ_3 to θ_2 to θ_4. For conciseness, the specific closed-form derivation of the joint angles are described briefly since they can be found in Ref. [19] and are not the focus of this paper. However, this paper does differentiate itself from prior work by expressing the formula in more explicit forms for ease of interpretation and reproducibility. θ_1 can be determined by analyzing the transformation from joint 1 to joint 5 and solving the corresponding phase-shift equation that results as follows.

$$\theta_1 = \arctan2(p_{0x}^5, p_{0y}^5) \pm \cos^{-1}\frac{d_4}{R_1^5} + \frac{\pi}{2} \tag{3}$$

where the following are explicitly expressed as

$$p_{0x}^5 = T_0^6(2,4) - d_6 T_0^6(2,3)$$

$$p_{0y}^5 = T_0^6(1,4) - d_6 T_0^6(1,3)$$

$$R_1^5 = \sqrt{(T_0^6(1,4) - d_6 T_0^6(1,3))^2 + (T_0^6(2,4) - d_6 T_0^6(2,3))^2}$$

Note that θ_1 has two possible solutions, and the recommended solution would be closest to the robot's initial position. By utilizing the transformation from joint 1 to joint 6 and Eq. (3), the following solution can be derived for θ_5.

$$\theta_5 = \pm\arccos\frac{T_0^6(1,4)\sin\theta_1 - T_0^6(2,4)\cos\theta_1 - d_4}{d_6} \tag{4}$$

By using a spherical transformation when describing the transformation from joint 1 to joint 6, θ_6 can be expressed as the follows:

$$\theta_6 = \arctan2\left(\frac{T_6^0(2,2)\cos\theta_1 - T_6^0(2,1)\sin\theta_1}{\sin\theta_5}, \frac{T_6^0(1,1)\sin\theta_1 - T_6^0(1,2)\cos\theta_1}{\sin\theta_5}\right) \tag{5}$$

Note that joints θ_3, θ_2, and θ_4 can be formulated from the standard planar RRR derivation [32]. Therefore, θ_3, θ_2, and θ_4 are formulated as follows:

$$\theta_3 = \pm\arccos\frac{R_1^{4^2} - a_2^2 - a_3^2}{2a_2a_3} \tag{6}$$

$$\theta_2 = \arctan2\left(-T_1^4(3,4),\ -T_1^4(1,4)\right) - \sin^{-1}\frac{-a_3\sin\theta_3}{R_1^4} \tag{7}$$

$$\theta_4 = \arctan2\left(T_3^4(2,1),\ T_3^4(1,1)\right) \tag{8}$$

where

$$R_1^4 = \sqrt{T_1^4(1,4)^2 + T_1^4(2,4)^2 + T_1^4(3,4)^2}$$

Thus, all the joint angles for the IK solution have been presented in an easy-to-interpret and explicit manner to be used in this work and future research. In addition, this derivation shows that errors in θ_1 will influence θ_5 and so on. Therefore, this paper will also examine error propagation throughout the IK solution for both the analytical and hybrid model.

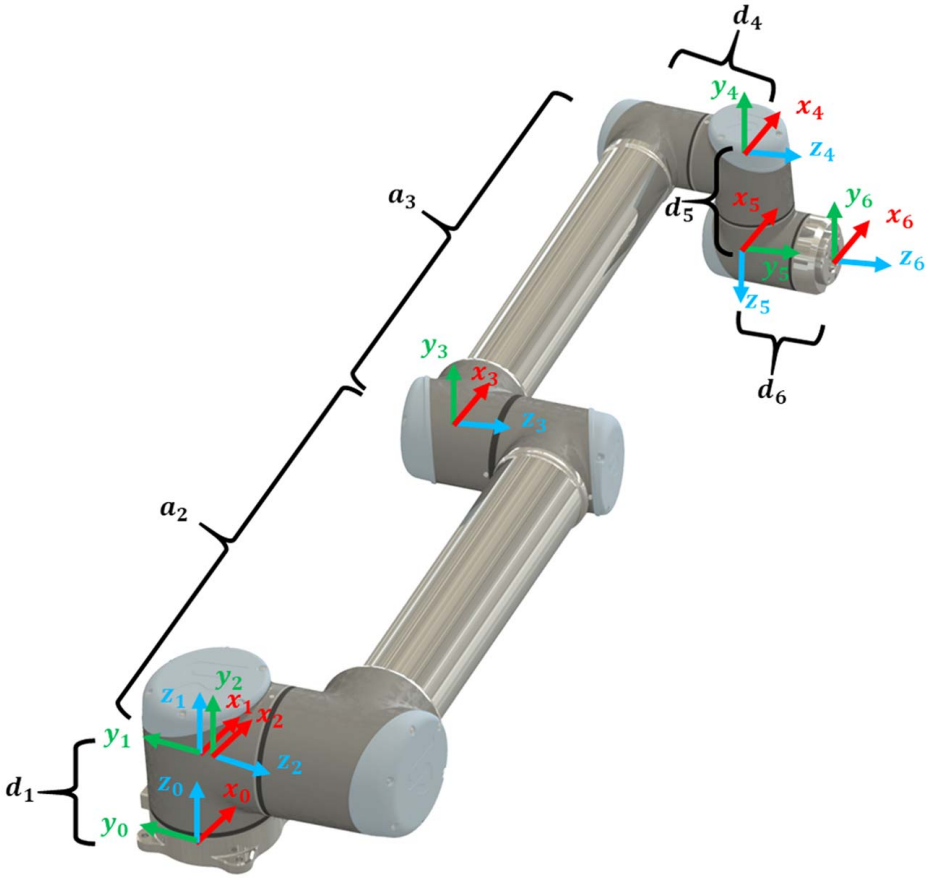

Fig. 1 Schematic of the Universal Robot arm

2.2 Bayesian Updating of Analytical Models. After the analytical functions have been established for both the FK and IK solutions, they can be treated as priors of a Gaussian process with posteriors that are formed after updating the model with more data. The general formulation of Bayesian updating is as follows. First, assume a Gaussian process as follows for an input datapoint x [33].

$$f(x) \sim GP(\beta(x), k(x, x')) \tag{9}$$

where $\beta(x)$ is the closed-form solution of the kinematic models treated as a mean function and $k(x, x')$ is the covariance function. In this work, the covariance function between two outputs is specified as

$$k(x_i, x_j) = \sigma_f^2 \exp \frac{-(x_i - x_j)^T (x_i - x_j)}{2\sigma_l^2} \tag{10}$$

where σ_l is the characteristic length scale and σ_f is the noise standard deviation. Note that Eq. (10) corresponds to a Bayesian linear regression model. In addition, the explicit covariance function implies a distribution over $\beta(x)$. Thus, training data from experiments can form a posterior distribution based from the assumed prior. Therefore, the joint distribution between the data output y_t and set of inputs X_t and the corresponding query function f_* for a query dataset X_* can be expressed as follows:

$$\begin{bmatrix} y_t \\ f_* \end{bmatrix} \sim N\left(0, \begin{bmatrix} K(X_t, X_t) + \sigma^2 \boldsymbol{I} & K(X_t, X_*) \\ K(X_*, X_t) & K(X_*, X_*) \end{bmatrix}\right) \tag{11}$$

where $K(X, X)$ is the covariance matrix with indices defined by Eq. (10) and σ^2 is the variance of the observations. Therefore, the output form of the Gaussian process given X, y_t, and X_* is defined as $N(\overline{f}_*, cov(f_*))$ where

$$\overline{f}_* = K(X_*, X)[K(X, X) + \sigma^2 \boldsymbol{I}]^{-1} y + \beta(X_*) \tag{12}$$

$$cov(f_*) = K(X_*, X_*) - K(X_*, X)[K(X, X) + \sigma^2 \boldsymbol{I}]^{-1} K(X, X_*) \tag{13}$$

Thus, Eq (12) is the output prediction of the hybrid model. Note that the computation of Eq. (12) is relatively inexpensive if $[K(X, X) + \sigma^2 \boldsymbol{I}]^{-1} y$, which is determined from the training dataset, is calculated beforehand. Therefore, this approach is suitable for applications with computation constraints such as real-time control when compared to alternate statistical methods [34]. Thus, this approach is feasible for small and medium sized industries and manufacturers that cannot leverage the capabilities of powerful computational hardware.

3 Experimental Setup

To evaluate the proposed hybrid model, experiments were conducted on UR5 and UR10 robots. In these experiments, the robot was driven to a set of random poses. At each position, the robot was stationary for two seconds while the joint angles were measured from the robot controller and the end effector position was measured with an Optitrack TRIO. To control the robot during the experiments, nominal joint angles were sent to the robot using User Datagram Protocol (UDP) protocol while the Optitrack TRIO data was recorded using the NatNet Software Development Kit (SDK). Five motion capture markers were mounted onto the robot end effector. The center marker was set as the pivot point of the tracked rigid body. The end effector was manufactured such that the center of the center marker was offset by 20 mm from the robot flange +Z direction. Thus, the center of the flange was tracked by offsetting the rigid body by 20 mm from its

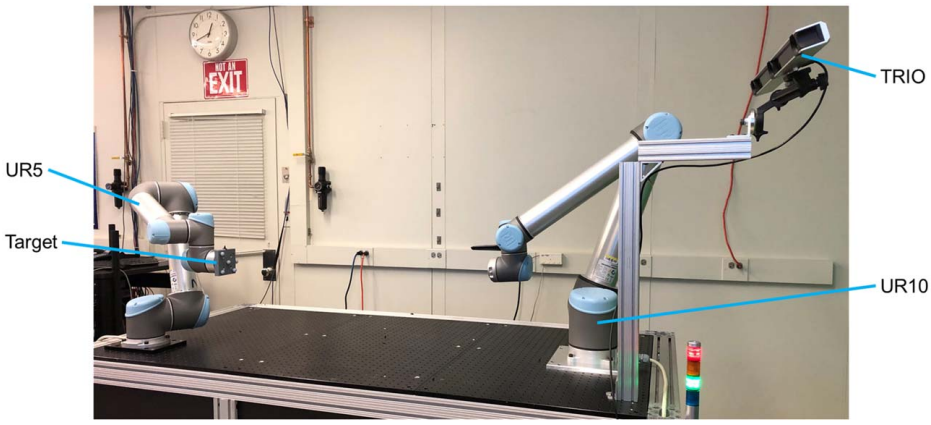

Fig. 2 Experimental setup for UR5 experiments. The TRIO was relocated to facilitate measurements for the UR10.

measured location. In addition, the five markers were used to calculate the orientation of the target, which was calibrated to be the same as the flange by initializing the R_x, R_y, and R_z of the rigid body target at the 0 deg, 0 deg, and 0 deg orientation, respectively, with respect to the robot's base frame. Note that the Optitrack TRIO was characterized using a scale bar test. The scale bar was placed 50, 100, 150, 200, 250, and 300 mm horizontally from the TRIO. The distance between the two markers on the scale bar (nominal length of 174.763 mm) was measured at each of the five positions. The average deviation was calculated to be 0.12 mm with a standard deviation of 0.084 mm. To register the Optitrack TRIO sensor frame to the robot frame, an efficient three-point registration technique was conducted. Using this registration technique, three points were measured in the robot frame and sensor frame to create an intermediate coordinate system from which the homogeneous transformation matrix between the robot base frame and sensor frame was computed [35]. Figure 2 shows the experimental setup. Note that this experimental setup can be used as a standardized testbed and methodology to evaluate performance of kinematic models for industrial robots.

The ranges of joint angles for the poses are shown in Table 1. Note that the joint angles used in this work were randomly generation from a uniform distribution to avoid possible experimental bias in the results. Note that the commanded joint sets were the same for the UR5 and UR10. In addition, note that uniformly sampling at a fairly coarse increment of 5 deg of the workspace listed in Table 1 would require 663,552 samples. Thus, model calibration would take approximately 530 h if sampling an average of 20.8 poses/min, which was the rate at which the experiments were conducted. Thus, these experiments already demonstrate the tedious nature of conducting only statistical methods to sample the workspace, which would be infeasible for small and medium sized industries. Thus, these experiments show the need for more efficient calibration methods of kinematic models.

Table 2 shows the DH parameters used in the analytical and hybrid models. Note that the DH parameters were specifically calibrated by driving the robot to known hold positions on a precision plate and recording the joint and end effector positions [36]. The procedure is then repeated at multiple positions on the plate. As shown in Eqs. (1) and (2), a system of equations can be developed with known Cartesian positions and joint angles and unknown DH parameters. By recording multiple poses, nonlinear least squares minimization is conducted to determine the change in DH parameters by starting the search at the original DH parameters [37].

The end result of the calibration procedure is the modification to the DH parameters that are also shown in Table 2. Note that the results of the calibration show that the change in parameters can be as large as 380.77 mm for UR5 d_2. However, note that the subsequent calibration correction factor (UR5 d_3) is −381.46 mm, which compensates for the extreme calibration factor in UR5 d_2. A consistent limitation of kinematic calibration is that the system of equations is significantly underdetermined due to six equations and 18 unknown DH parameters. Therefore, Table 2 shows that calibrating DH parameters used in analytical models can result in coefficients with nonsensical physical meanings. In addition, even if the calibration is "perfect," the fundamental equation forms of the kinematics can be erroneous due to failure to consider effects including backlash.

Table 1 Joint angle bounds for experiments (all units in degrees)

	θ_1	θ_2	θ_3	θ_4	θ_5	θ_6
min	60	−100	70	−10	40	40
max	100	−60	100	50	100	100

4 Results

In this work, the hybrid modeling approach was compared to the previously described analytical models and a Gaussian process with no prior distribution (labeled as "no prior"), which represents a purely statistical model approach that is commonly used in applications including pose prediction of continuum robots [38] and robotic learning by demonstration [39]. In addition, another purely statistical model that was studied in this work was a neural network model, which has been demonstrated to be used in prior kinematic modeling [29–31]. In this work, the neural network was configured to be a single layer, 10 neuron neural network with a rectified linear unit activation function. Also, the hybrid model using calibrated DH parameters was compared to a hybrid model without using the corrected DH parameters. The performance of the models with respect to solving the FK problem is first described followed by the IK problem. 250, 500, 750, and 1000 calibration poses were tested to evaluate the performance of the models in the presence of increasing data. For the hybrid, no prior, and neural network models, a five-fold cross-validation approach was conducted with the root-mean-squared error (RMSE) calculated as the metric of model accuracy. Because the analytical model uses factory-calibrated coefficients, the RMSE was computed using the full dataset with no cross-validation. In addition, as the closed-form IK solution is solved sequentially, error propagation is explored to provide fundamental understanding of the influence of the sequential errors in both the analytical and hybrid models.

Table 2 Nominal and calibrated modifying factors DH Parameters for UR5 and UR10 Robot

	UR5						UR10					
i	a_i	Δa_i	d_i	Δd_i	α_i	$\Delta\alpha_i$	a_i	Δa_i	d_i	Δd_i	α_i	$\Delta\alpha_i$
1	0	2.27×10^{-4}	89.16	1.08×10^{-4}	$\pi/2$	-2.81×10^{-4}	0	2.03×10^{-5}	127.30	6.7×10^{-4}	$\pi/2$	-3.55×10^{-4}
2	−425	0.34	0	380.77	0	1.09×10^{-3}	−612	2.72×10^{-3}	0	8.52	0	-7.27×10^{-3}
3	−392.25	1.03×10^{-4}	0	−381.46	0	7.97×10^{-3}	−572.30	1.89×10^{-3}	0	−10.92	0	−0.01
4	0	-3.36×10^{-4}	109.15	0.68	$\pi/2$	-8.22×10^{-4}	0	-3.88×10^{-4}	163.94	2.41	$\pi/2$	-9.39×10^{-4}
5	0	4.55×10^{-4}	94.65	-2.26×10^{-5}	$-\pi/2$	4.53×10^{-4}	0	4.43×10^{-4}	115.70	-8.17×10^{-5}	-$\pi/2$	3.69×10^{-4}
6	0	0	82.30	4.01×10^{-5}	0	0	0	0	92.20	1.82×10^{-4}	0	0

Note: The units for a, d, and α are mm, mm, and radians, respectively.

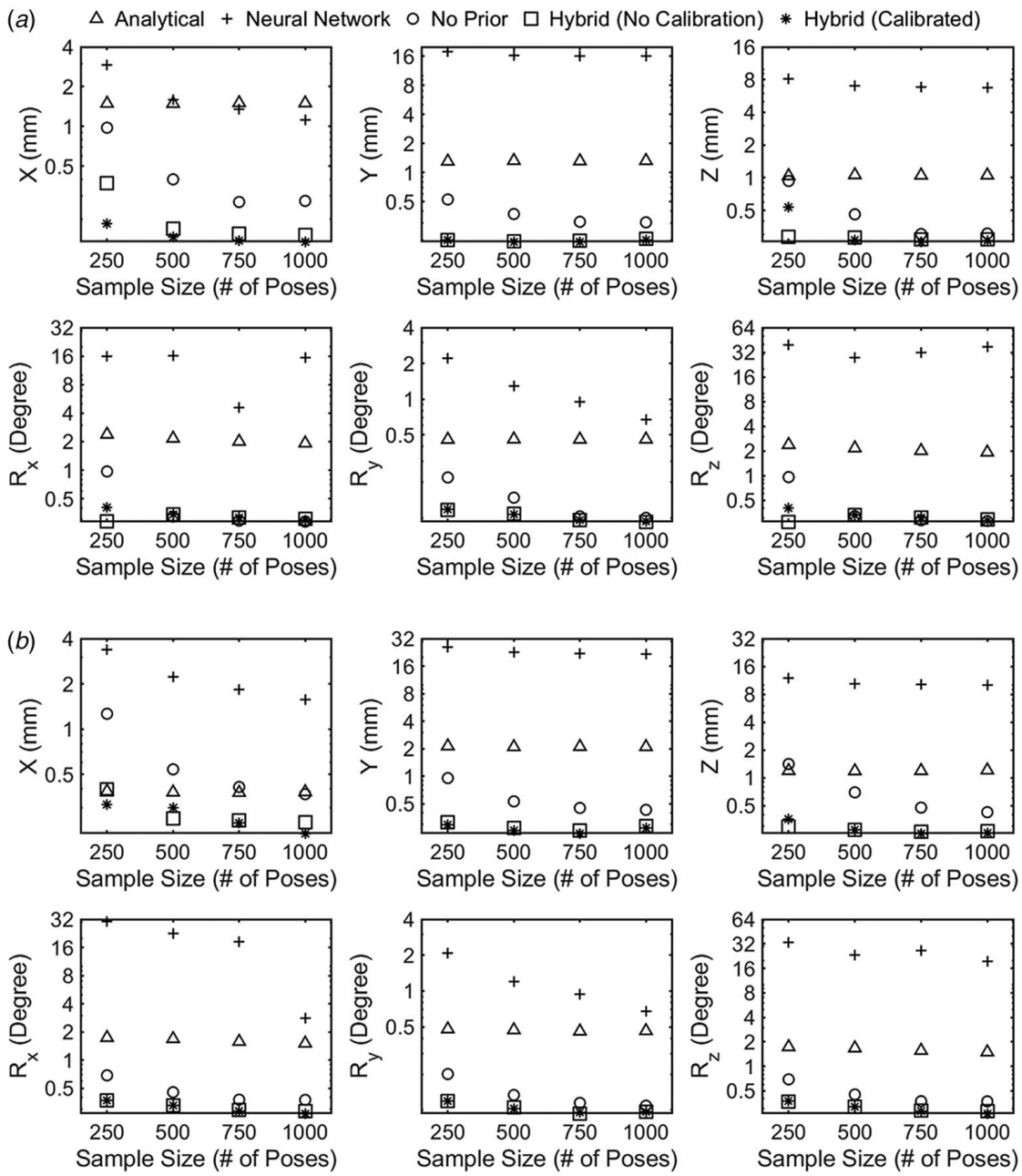

Fig. 3 FK RMSE for (*a*) UR5 and (*b*) UR10

4.1 Forward Kinematics. The outputs of all models were represented as homogeneous transformation matrices in Eq. (2). The rotation matrix notation was converted to Euler angles, while the positional coordinates were extracted from the last column of the homogeneous transformation matrix to compare with direct measurements from the TRIO. Figure 3 shows the RMSE for the analytical, neural network, hybrid, and purely statistical with no prior models.

The RMSE values for all the analytical model predictions are shown to be invariant with respect to sample size. This is expected since the DH parameters in the analytical models were factory-calibrated. In addition, the invariance to the sample size shows that the quality of the data itself is consistent regardless of sample size (i.e., no region in the workspace appears too densely sampled). Interesting to note is that the no prior and neural network models tend to experience convergence from a large RMSE to a smaller RMSE as the sample size increases. For example, the RMSE of the no prior model for the UR5 X position prediction is initially 0.98 mm at 250 sample poses. Then the RMSE converges to 0.27 mm at 1000 sample poses as more points are added to the model. Thus, the number of sampled points is important for calibration of purely statistical models. However, the density of points for a given workspace for a statistical model to achieve a desired RMSE is extremely difficult for small and medium sized industries to determine without extensive and iterative experiments. In addition, the hybrid model also exhibits convergence, such as in the prediction of the UR10 Z position (starting at 0.54 mm and ending at 0.26 mm). However, the severity of the convergence is much less than the purely statistical models, which shows that the hybrid model does not have such a large reliance on the amount of data relative to the statistical model. Hence, the hybrid model is shown to outperform the analytical, neural network, and no prior models to solve the FK problem. In addition, the hybrid model without calibration performs similarly with

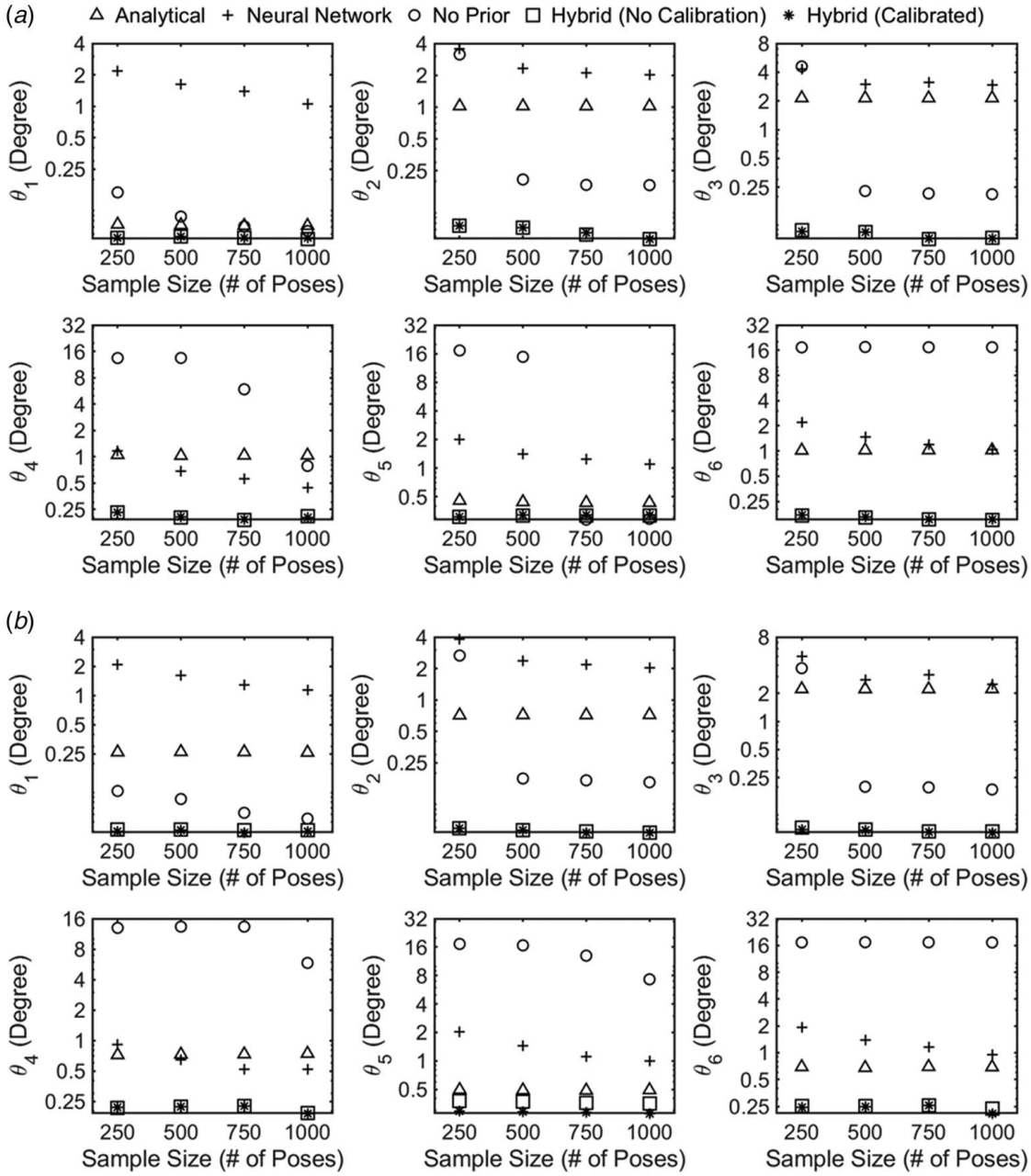

Fig. 4 IK RMSE for (*a*) UR5 and (*b*) UR10

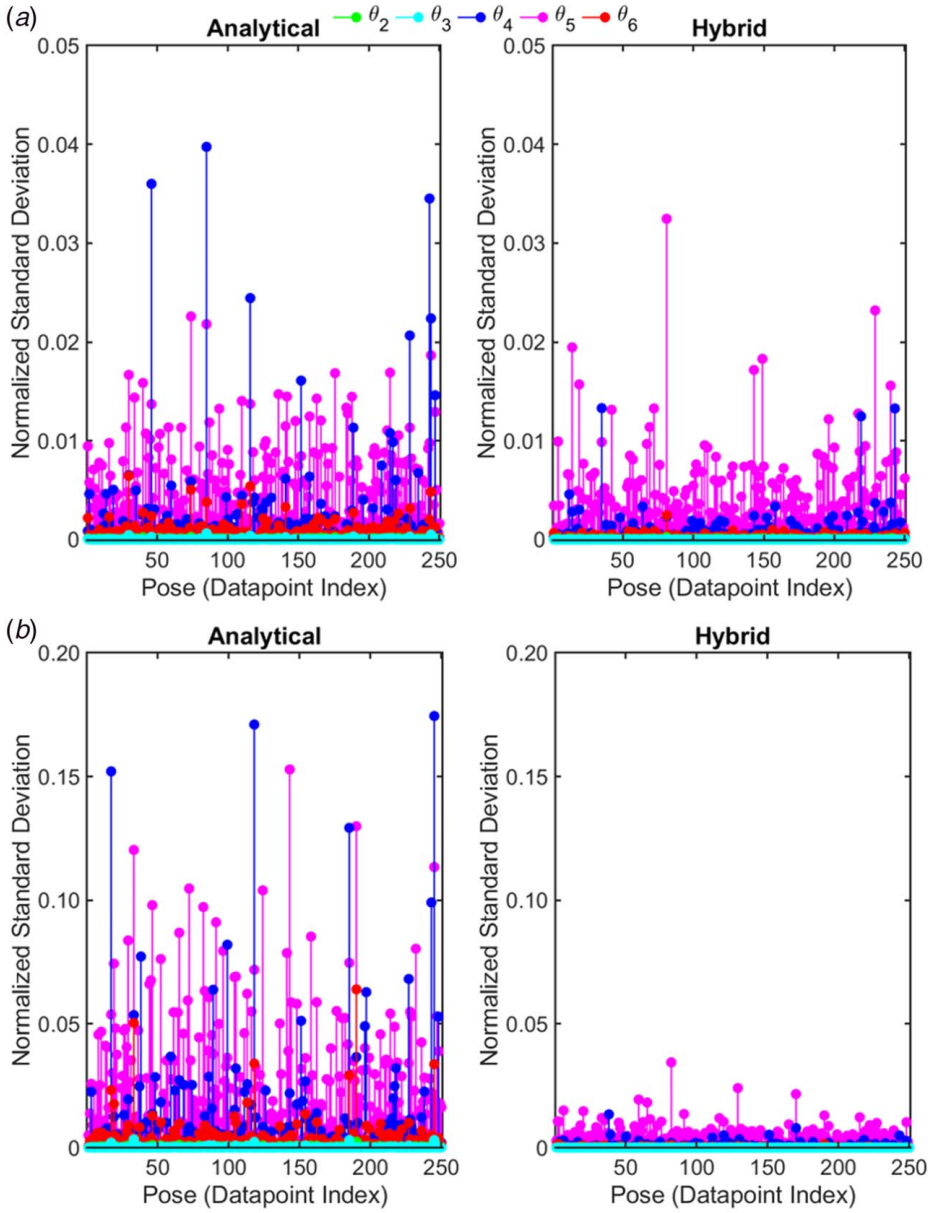

Fig. 5 Monte Carlo Standard Deviation Results for (*a*) UR5 and (*b*) UR10

calibration, thus demonstrating that the hybrid model may not require a calibration procedure for accurate predictions.

Figure 3 also shows that at final convergence, the neural network and analytical models perform poorly. This is because the analytical model does not account for the influence of outside factors, such as gear backlash, that are captured by the TRIO measurements, and the neural network model uses a covariance matrix in its output formulation and therefore is heavily dependent on the number of datapoints used in its training. Overall, the no prior model performs similar to the hybrid model in predicting the Euler angles after convergence. However, the no prior model RMSE appears to converge at an offset larger than the hybrid model in the X, Y, and Z positions. For instance, the UR10 Y direction RMSE converges at 0.43 mm and 0.27 mm for the no prior and hybrid models, respectively. This implies that even after an extensive number of points are sampled, the hybrid model will still outperform the purely statistical models. It is also interesting to note that the analytical model shows fairly accurate predictions even though the modification to the DH parameters are extremely large as shown and discussed previously in Table 2. This shows that the factory calibration of the

Table 3 Average normalized standard deviation among all simulations

	UR5					UR10				
	θ_2	θ_3	θ_4	θ_5	θ_6	θ_2	θ_3	θ_4	θ_5	θ_6
Analytical	0.07	0.03	2.05	5.54	0.69	0.32	0.14	10.75	28.95	3.52
Hybrid	0.05	0.01	0.07	4.20	0.22	0.04	0.005	0.68	4.26	0.17

Note: All units are in kilodegree/degree.

DH-parameters does indeed result in a more accurate performance even though the physical meanings of the correction factors are not intuitive.

4.2 Inverse Kinematics. Figure 4 shows the IK RMSE for the analytical, neural network, no prior, and hybrid models. Similar to the FK results, the analytical model RMSE is shown to be invariant to the number of data samples. In addition, note that the RMSE for the no prior model does not even appear to converge for θ_6 and takes substantially more points to converge for θ_4 compared to the FK results. In addition, the neural network is shown to perform better than the no prior model for the θ_4, θ_5, and θ_6 predictions. This is because the IK problem is much more nonlinear compared to the FK problem owing to multiple solutions and discontinuities resulting from inverse tangent operations. Therefore, the no prior model will require many more points to lower the RMSE to an acceptable level while the neural network model would require less points than the no prior model. It is also interesting to note that the IK hybrid model does not appear to converge as much as its FK counterpart. This could be because the hybrid model is based on an already nonlinear prior mean function, and therefore not as much data is required to convergence to capture the nonlinear behavior.

Overall, the calibrated hybrid model is shown to have the lowest RMSE for the IK predictions with similar results as the hybrid model with no calibration, thus demonstrating that calibration may not be required for either the FK or IK solutions. Overall, the analytical model performs decently, but some of the RMSE values are unacceptable in certain high-precision applications, such as machining and fastening, compared to the hybrid model. For instance, the converged RMSE for the UR10 θ_1 for the statistical and hybrid models are 0.26 deg and 0.04 deg, respectively. In addition, the neural network and no prior models are shown to perform worst out of all the models and would therefore require more datapoints for calibration.

4.3 Error Propagation. As stated previously, the order of calculating the joint angles for the analytical and hybrid IK solutions is θ_1, θ_5, θ_6, θ_3, θ_2, and θ_4. Therefore, an error in calculating θ_1 will influence all subsequent calculations. Thus, it is important to study the influence of error propagation for both the analytical and hybrid model. Specifically, this paper uses a Monte Carlo simulation to study the influence of error propagation. Initially, a known value of θ_1 is sampled from the dataset. The value of θ_1 is assumed to be the mean of a normally distributed variable. The standard deviation of the distribution is the RMSE determined from Fig. 4. Thus, a sample from the distribution of θ_1 is then used as an input to calculate θ_5. The values of θ_1 and θ_5 are then used to predict θ_6. Note that because θ_5 only depends on θ_1, the same number of θ_5 and θ_1 solutions is calculated. Hence, the procedure for the simulation is as follows:

(1) Compute θ_1 distribution using RMSE from Fig. 4
(2) Sample from θ_1 distribution to calculate θ_5 distribution
(3) Sample from θ_1 and θ_5 distributions to calculate θ_6 distribution
(4) Sample from θ_1, θ_5, and θ_6 distributions to calculate θ_3 distribution
(5) Sample from θ_1, θ_5, θ_6, and θ_3 distributions to calculate θ_2 distribution
(6) Sample from θ_1, θ_5, θ_6, θ_3, and θ_2 distributions to calculate θ_4 distribution

However, because θ_6 depends on θ_1 and θ_5, all combinations of θ_1 and θ_5 are sampled (resulting in a number of θ_6 calculations that is equal to the number of θ_1 calculations squared). Thus, it can be seen that the simulation can become costly. The size of the dataset used in the simulation is therefore limited to 250 points. The quantifying metric to determine the influence of error propagation is the standard deviation of the calculated joint angles. Thus, if a large standard deviation results from a particular joint calculation, then the influence of the error propagation is assumed to be large.

Figure 5 shows the normalized standard deviation calculated by the error propagation simulation. Figure 5 shows that θ_4 and θ_5 tend to experience the largest normalized standard deviations. Interestingly, θ_5 and θ_4 are the first and last variables to be solved after θ_1 is initially computed. Thus, it appears that the forms of Eqs. (3)–(8) are more important to determining which joints in the analytical and hybrid models are more susceptible to error propagation as opposed to the order in which the joint angles are calculated. For instance, Eq. (8) shows that θ_4 exhibits less addition/subtraction operations that could have minimized perturbations in the final output. Also, Eq. (4) conducts the inverse cosine operation, which can amplify the influence of θ_1 on the output. In addition, it appears that the UR10 joints experience larger normalized standard deviation with respect to analytical model errors than the UR5. This is because the UR10 is a larger robot, and therefore error in the analytical model will influence the analytical IK solution to a larger degree.

Table 3 shows the normalized standard deviation averaged among all simulations. Interestingly, the hybrid model is shown to reduce the normalized standard deviation for θ_4, but θ_5 is shown to exhibit the largest normalized standard deviation for both models and both robots. This may be due to the wrist singularities resulting from θ_4 and θ_5 compensating for each other. Thus, the hybrid model may be able to compensate for these singularities more. This reinforces the notion that the error propagation of the IK solutions are more reliant on the equation form than their order of solutions. In addition, Table 3 shows that the hybrid model results in smaller normalized standard deviations compared to the analytical model. This is because the hybrid model is more tuned to the data than the analytical model, and therefore, variations in the inputs will have less influence on the uncertainty of the output. Therefore, the hybrid IK model is shown to be more robust to propagation errors than the analytical IK model.

5 Conclusion

This paper describes, develops, and experimentally validates a hybrid analytical and statistical modeling approach to predicting the FK and IK solutions of industrial robots. By treating the analytical model as a known prior mean function in a Gaussian process, Bayesian inference is used to update the Gaussian process with experimental data. A generalized pose-measuring testbed and methodology using the Optitrack TRIO and randomized robot poses was used to evaluate the analytical, neural network, no prior, and hybrid models for UR5 and UR10 robots. The hybrid model was shown to result in the lowest RMSE compared to all the models. In addition, the hybrid model was shown to perform similarly without DH parameter calibration and therefore this model may not require the calibration procedure. A Monte Carlo simulation was studied to explore the influence of error propagation on the IK solutions. It was shown that the error propagation was more dependent on the equation form than the sequence of equations. In addition, the hybrid IK model was shown to be more robust to error propagation than the analytical IK model.

Using the general pose testbed methodology in this work, more robot types can be tested. However, note that the hybrid approach in this paper is primarily focused on using closed-form solutions that are available for UR5 and UR10 robots. Future work is required to explore methods to conduct Bayesian updating on numerical methods, such as the iterative Jacobian approach, for more complex robot types, such as the ABB YuMi. In addition, more modeling and calibration methods can be evaluated using the testbed and the dataset provided in this work. Also, this general testbed methodology can be used to study the influence of performance degradation of industrial robots, particularly because the hybrid model in this work can be continuously calculated during robot operation.

Acknowledgment

This work was funded by the National Institute of Standards and Technology and the National Research Council Research Associateship Program.

Disclaimer

Certain commercial equipment, instruments, or materials are identified in this paper in order to specify the experimental procedure adequately. Such identification is not intended to imply recommendation or endorsement by NIST, nor is it intended to imply that the materials or equipment identified are necessarily the best available for the purpose.

Conflict of Interest

There are no conflicts of interest.

Data Availability Statement

The data and information that support the findings of this article are freely available.[2] The authors attest that all data for this study are included in the paper. Data provided by a third party listed in Acknowledgment.

References

[1] Sen, D. K., Datta, S., Patel, S. K., and Mahapatra, S. S., 2015, "Multi-Criteria Decision Making Towards Selection of Industrial Robot," Bench.: Int. J., **22**(3), pp. 465–487.
[2] Singh, S., Singla, A., Singh, A., Soni, S., and Verma, S., 2016, "Kinematic Modelling of a Five-DOFs Spatial Manipulator Used in Robot-Assisted Surgery," Perspect. Sci., **8**, pp. 550–553.
[3] Dahari, M., and Tan, J.-D., 2011, "Forward and Inverse Kinematics Model for Robotic Welding Process Using Kr-16ks Kuka Robot," 2011 Fourth International Conference on Modeling, Simulation and Applied Optimization, IEEE, pp. 1–6.
[4] Kaldestad, K. B., Tyapin, I., and Hovland, G., 2015, "Robotic Face Milling Path Correction and Vibration Reduction," 2015 IEEE International Conference on Advanced Intelligent Mechatronics (AIM), IEEE, pp. 543–548.
[5] Kim, C., Espalin, D., Cuaron, A., Perez, M. A., Lee, M., MacDonald, E., and Wicker, R. B., 2015, "Cooperative Tool Path Planning for Wire Embedding on Additively Manufactured Curved Surfaces Using Robot Kinematics," ASME J. Mech. Rob., **7**(2), p. 021003.
[6] Manocha, D., and Canny, J. F., 1994, "Efficient Inverse Kinematics for General 6r Manipulators," IEEE. Trans. Rob. Autom., **10**(5), pp. 648–657.
[7] Liu, Y., Kong, M., Wan, N., and Ben-Tzvi, P., 2018, "A Geometric Approach to Obtain the Closed-Form Forward Kinematics of H4 Parallel Robot," ASME J. Mech. Rob., **10**(5), p. 051013.
[8] López-Custodio, P., Dai, J., Fu, R., and Jin, Y., 2020, "Kinematics and Constraints of the Exechon Robot Accounting Offsets Due to Errors in the Base Joint Axes," ASME J. Mech. Rob., **12**(2), p. 021109.
[9] Chesser, P. C., Wang, P. L., Vaughan, J. E., Lind, R. F., and Post, B. K., 2021, "Kinematics of a Cable-Driven Robotic Platform for Large-Scale Additive Manufacturing," ASME J. Mech. Rob., **14**(2), p. 021010.
[10] Wang, L., Del Giudice, G., and Simaan, N., 2019, "Simplified Kinematics of Continuum Robot Equilibrium Modulation Via Moment Coupling Effects and Model Calibration," J. Mech. Rob., **11**(5), p. 44162.
[11] Spong, M. W., Hutchinson, S., and Vidyasagar, M., 2006, Robot Modeling and Control.
[12] Patil, A., Kulkarni, M., and Aswale, A., 2017, "Analysis of the Inverse Kinematics for 5 DOF Robot Arm Using Dh Parameters," 2017 IEEE International Conference on Real-time Computing and Robotics (RCAR), IEEE, pp. 688–693.
[13] Jiang, Z., Zhou, W., Li, H., Mo, Y., Ni, W., and Huang, Q., 2017, "A New Kind of Accurate Calibration Method for Robotic Kinematic Parameters Based on the Extended Kalman and Particle Filter Algorithm," IEEE. Trans. Ind. Electron., **65**(4), pp. 3337–3345.
[14] Ranjan, A., Kumar, U., Laxmi, V., and Udai, A. D., 2017, "Identification and Control of NAO Humanoid Robot to Grasp An Object Using Monocular Vision," 2017 Second International Conference on Electrical, Computer and Communication Technologies (ICECCT), IEEE, pp. 1–5.
[15] Zhou, J., Nguyen, H.-N., and Kang, H.-J., 2014, "Simultaneous Identification of Joint Compliance and Kinematic Parameters of Industrial Robots," Int. J. Precis. Eng. Manuf., **15**(11), pp. 2257–2264.
[16] He, J., Gao, F., and Sun, Q., 2019, "Design and Kinematic Analysis of a Novel Hybrid Kinematic Mechanism with Seven-degrees-of-freedom and Variable Topology for Operation in Space," ASME J. Mech. Rob., **11**(1), p. 011003.
[17] Cohen, A., and Shoham, M., 2016, "Application of Hyper-dual Numbers to Multibody Kinematics," ASME J. Mech. Rob., **8**(1), p. 011015.
[18] Sun, J.-D., Cao, G.-Z., Li, W.-B., Liang, Y.-X., and Huang, S.-D., 2017, "Analytical Inverse Kinematic Solution Using the Dh Method for a 6-DOF Robot," 2017 14th International Conference on Ubiquitous Robots and Ambient Intelligence (URAI), IEEE, pp. 714–716.
[19] Kebria, P. M., Al-Wais, S., Abdi, H., and Nahavandi, S., 2016, "Kinematic and Dynamic Modelling of Ur5 Manipulator," 2016 IEEE International Conference on Systems, Man, and Cybernetics (SMC), IEEE, p. 004229.
[20] Duleba, I., and Opalka, M., 2013, "A Comparison of Jacobian-based Methods of Inverse Kinematics for Serial Robot Manipulators," Int. J. Appl. Math. Comput. Sci., **23**(2), pp. 373–382.
[21] Colomé, A., and Torras, C., 2014, "Closed-loop Inverse Kinematics for Redundant Robots: Comparative Assessment and Two Enhancements," IEEE/ASME Trans. Mech., **20**(2), pp. 944–955.
[22] Fu, Z., Yang, W., and Yang, Z., 2013, "Solution of Inverse Kinematics for 6r Robot Manipulators with Offset Wrist Based on Geometric Algebra," J. Mech. Rob., **5**(3), p. 0310081.
[23] Ferrentino, E., and Chiacchio, P., 2020, "On the Optimal Resolution of Inverse Kinematics for Redundant Manipulators Using a Topological Analysis," ASME J. Mech. Rob., **12**(3), p. 031002.
[24] Conrad, K. L., Shiakolas, P. S., and Yih, T., 2000, "Robotic Calibration Issues: Accuracy, Repeatability and Calibration," Proceedings of the 8th Mediterranean Conference on Control and Automation (MED2000), Rio, Patras, Greece, Vol. 1719.
[25] Ruderman, M., Hoffmann, F., and Bertram, T., 2009, "Modeling and Identification of Elastic Robot Joints With Hysteresis and Backlash," IEEE. Trans. Ind. Electron., **56**(10), pp. 3840–3847.
[26] Shalev-Shwartz, S., and Ben-David, S., 2014, *Understanding Machine Learning: From Theory to Algorithms*, Cambridge University Press, New York.
[27] Dereli, S., and Köker, R., 2020, "A Meta-Heuristic Proposal for Inverse Kinematics Solution of 7-DOF Serial Robotic Manipulator: Quantum Behaved Particle Swarm Algorithm," Artificial Intel. Rev., **53**(2), pp. 949–964.
[28] Raja, R., Dutta, A., and Dasgupta, B., 2019, "Learning Framework for Inverse Kinematics of a Highly Redundant Mobile Manipulator," Rob. Auton. Syst., **120**, p. 103245.
[29] Alebooyeh, M., and Urbanic, R. J., 2019, "Neural Network Model for Identifying Workspace, Forward and Inverse Kinematics of the 7-DOF YuMi 14000 Abb Collaborative Robot," IFAC-PapersOnLine, **52**(10), pp. 176–181.
[30] Reinhart, R. F., Shareef, Z., and Steil, J. J., 2017, "Hybrid Analytical and Data-Driven Modeling for Feed-Forward Robot Control," Sensors, **17**(2), p. 311.
[31] Chen, J., and Lau, H. Y., 2016, "Inverse Kinematics Learning for Redundant Robot Manipulators with Blending of Support Vector Regression Machines," 2016 IEEE Workshop on Advanced Robotics and its Social Impacts (ARSO), IEEE, pp. 267–272.
[32] Wu, J., Wang, J., Wang, L., and You, Z., 2010, "Performance Comparison of Three Planar 3-dof Parallel Manipulators With 4-rrr, 3-rrr and 2-rrr Structures," Mechatronics, **20**(4), pp. 510–517.
[33] Rasmussen, C. E., 2003, "Gaussian Processes in Machine Learning," *Summer School on Machine Learning*, MIT Press, Boston, MA, pp. 63–71.
[34] Zhou, Z., Ong, Y. S., Nguyen, M. H., and Lim, D., 2005, "A Study on Polynomial Regression and Gaussian Process Global Surrogate Model in Hierarchical Surrogate-assisted Evolutionary Algorithm," 2005 IEEE Congress on Evolutionary Computation, Vol. 3, IEEE, pp. 2832–2839.
[35] Marvel, J. A., and Van Wyk, K., 2016, "Simplified Framework for Robot Coordinate Registration for Manufacturing Applications," 2016 IEEE International Symposium on Assembly and Manufacturing (ISAM), pp. 56–63.
[36] Universal Robot, 2019. *Kinematic Calibration Manual for e-Series*.
[37] Dennis Jr, J. E., Gay, D. M., and Walsh, R. E., 1981, "An Adaptive Nonlinear Least-squares Algorithm," ACM Trans. Mathe. Soft. (TOMS), **7**(3), pp. 348–368.
[38] Fang, G., Wang, X., Wang, K., Lee, K.-H., Ho, J. D., Fu, H.-C., Fu, D. K. C., and Kwok, K.-W., 2019, "Vision-based Online Learning Kinematic Control for Soft Robots Using Local Gaussian Process Regression," IEEE Rob. Auto. Lett., **4**(2), pp. 1194–1201.
[39] Schneider, M., and Ertel, W., 2010, "Robot Learning by Demonstration With Local Gaussian Process Regression," 2010 IEEE/RSJ International Conference on Intelligent Robots and Systems, Taipei, Taiwan, Oct. 18–22, IEEE, pp. 255–260.

[2]https://github.com/vnguyen43/Hybrid˙Robot˙Kinematic˙Model